PCCP

CrossMark
← click for updates

Effects of atomic interaction stiffness on low-temperature relaxation of amorphous solids†

Y. T. Sun,[a] J. Q. Wang,[ab] Y. Z. Li,[a] H. Y. Bai,[a] M. Z. Li*[c] and W. H. Wang*[a]

While low-temperature relaxations show significant differences among metallic glasses with different compositions, the underlying mechanism remains mysterious. Using molecular dynamics simulation, low-temperature relaxation of amorphous solids is investigated in model systems with different atomic interaction stiffness. It was found that as the interaction stiffness increases, the low-temperature relaxation is enhanced. The fraction of mobile atoms increases with increasing interaction stiffness, while the length scale of dynamical heterogeneity does not change. The enhanced relaxation may be due to increased dynamical heterogeneity. These findings provide a physical picture for better understanding the origin of low-temperature relaxation dynamics in amorphous solids, and the experimentally observed different β-relaxation behaviors in various metallic glasses.

I. Introduction

The relaxation dynamics of a material can be well illustrated in a dynamical mechanical spectrum (DMS), which is often considered as the fingerprint of the material's dynamical properties.[1–4] When cooling down to a glassy state, the α-relaxation in metallic glasses (MGs) is fully arrested and the β-relaxation dominates the relaxation dynamics, often exhibiting excess wings or peaks (for some compositions) in DMS.[5] β-Relaxation has been studied in various materials *via* different methods.[6,7] It is now widely accepted that the so called 'shoulders' or 'excess wings' also share the same nature with β-relaxation peaks, with difference in the strength of the relaxation dynamics.[2,8] β-Relaxation in MGs has been massively studied and found to be related to many mechanical properties.[9–11] It is generally believed that β-relaxation originates from local rearrangements of atoms, which are considered as elementary relaxation events in the thermally or stress activated processes.[12–15] However, a link between local atomic rearrangements and the experimentally observed β-relaxation in metallic glasses (MGs) is still lacking, which limits our understanding of the relaxation dynamics of MGs, especially in temperature regions well below glass transition temperature (T_g).[11]

β-Relaxation in MGs is most commonly experimentally studied *via* dynamical mechanical analysis (DMA), which reveals the internal friction of a material.[2,16] DMA measures the elastic and viscous nature of a material, with the value of phase difference $δ$ or loss modulus E'' as the indicator of relaxation dynamics. One of the most important features of β-relaxation in MGs is its compositional dependence nature.[17] Pronounced β-relaxation peaks are most likely to be found in rare earth (RE) based MGs.[2,18–20] This indicates that low-temperature relaxation behavior of MGs depends most significantly upon the interaction between atoms.

Molecular dynamics (MD) simulation can investigate the relation between individual atomic motions and internal friction of the whole system.[21] There have been substantial MD studies on the fast β-relaxation in supercooled liquids, which consider β-relaxation as some very short time atomic motions that correspond to the plateau in the mean-square displacements (MSD) or other physical quantities.[22,23] The study on β-relaxation in glassy systems requires going into temperature regions far below T_g, where the time scale of relaxation dynamics is too long and far beyond the typical timescale in the conventional MD simulations.[15] The recently developed MD-DMA method, which mimics the experimental DMA process, provides an effective way to directly investigate the long timescale relaxation dynamics in a wide temperature range well below T_g.[21,22]

In this work, we used the MD-DMA method to investigate low-temperature relaxation dynamics in various amorphous systems by changing the atomic interaction stiffness. It is found that as interaction stiffness increases, low-temperature relaxation dynamics is enhanced. This is mainly because the dynamics becomes more heterogeneous in amorphous systems with increasing interaction stiffness. However, the length scale

[a] *Institute of Physics, Chinese Academy of Sciences, Beijing 100190, P. R. China. E-mail: whw@iphy.ac.cn*

[b] *Key Laboratory of Magnetic Materials and Devices and Zhejiang Province Key Laboratory of Magnetic Materials and Application Technology, Ningbo Institute of Industrial Technology, Chinese Academy of Sciences, Zhejiang 315201, P. R. China*

[c] *Department of Physics, Beijing Key Laboratory of Opto-electronic Functional Materials & Micro-nano Devices, Renmin University of China, Beijing 100872, P. R. China. E-mail: maozhili@ruc.edu.cn*

† Electronic supplementary information (ESI) available. See DOI: 10.1039/c6cp04238d

This journal is © the Owner Societies 2016

Phys. Chem. Chem. Phys., 2016, **18**, 26643–26650 | 26643

of dynamical heterogeneity remains unchanged. Such relations between atomic interaction stiffness and relaxation dynamics are used to explain the experimental results that rare earth (RE) based MGs, whose interaction stiffness is estimated from the power law relation between the bulk modulus K and average molar volume V_m, generally possess stronger β-relaxation. The results could help us to construct a more thorough physical picture for understanding the dynamical properties of amorphous solids.

II. Models and simulation procedures

The models studied here are binary mixtures of Lennard-Jones particles, type A (8000) and type B (2000), with their interactions following eqn (1),

$$\begin{cases} E = 4\varepsilon_{\alpha\beta} \left[\left(\dfrac{\sigma_{\alpha\beta}}{r \cdot 2^{\frac{1}{a}}} \right)^{2a} - \left(\dfrac{\sigma_{\alpha\beta}}{r \cdot 2^{\frac{1}{a}}} \right)^{a} \right] & (r < \sigma_{\alpha\beta}) \\[2em] E = 4\varepsilon_{\alpha\beta} \left[\left(\dfrac{\sigma_{\alpha\beta}}{r \cdot 2^{\frac{1}{b}}} \right)^{2b} - \left(\dfrac{\sigma_{\alpha\beta}}{r \cdot 2^{\frac{1}{b}}} \right)^{b} \right] & (r > \sigma_{\alpha\beta}) \end{cases}, \quad (1)$$

where $\alpha, \beta \in \{A, B\}$ and parameters a, b indicate the stiffness of atomic interaction in the repulsive part and attractive part, respectively. Here, the difference between particle A and B are $\varepsilon_{aa} = 1$, $\varepsilon_{AB} = 1.5$, $\varepsilon_{BB} = 0.5$, $\sigma_{AA} = 1$, $\sigma_{AB} = 0.8$, $\sigma_{BB} = 0.88$. To investigate the effects of atomic interaction stiffness, parameters a, b are selected to be 6-6, 6-9, 6-12, 9-6, 12-6, 9-9, and 12-12, respectively, which indicates the 7 different models studied in this work. For computational efficiency these model potentials were truncated and shifted at a distance of $2.5\sigma_{\alpha\beta}$. All units in this article are reduced L-J units. Thus, the energy minimum of interatomic potentials remains at $r_{min} = 1$ and $E_{min} = -1$, while the stiffness of interaction changes with the choice of a and b. Fig. 1(a) shows the interatomic potentials of A atoms in the seven model systems. The atomic interactions in the repulsive and attractive region are tuned separately. The 6-6 potential is similar to the well-studied Kob–Andersen (KA) model.[24,25]

Samples are obtained by fast cooling from equilibrium high temperature liquids with the same cooling rate of 2×10^3, and then annealed at designated temperatures. MD-DMA processes were then performed on these samples, during which a sinusoidal shear strain $\varepsilon(t) = \varepsilon_A \sin(2\pi t/T_\omega)$ is applied along xy direction with a maximum strain ε_A of 2%, within the elastic limit. Please see Methods for details of the sample preparations and MD-DMA processes.[26,27] The respond stress is fitted in terms of $\sigma(t) = \sigma_0 + \sigma_A \sin(2\pi t/T_\omega + \delta)$, where σ_0 is a small linear term, and δ is the phase difference between stress and strain. The storage (E') and loss modulus (E'') can be calculated by $E' = \sigma_A/\varepsilon_A \cos(\delta)$ and $E'' = \sigma_A/\varepsilon_A \sin(\delta)$, respectively. See ESI† Section S1 for more details of simulation procedure.

III. Results and discussions

### A. Structural information of the models

Models with different atomic interaction stiffness under the same sample preparation processes show similar structures. The pair correlation functions (PCF) of all systems at $T = 0.01$ and 0.55 are shown in Fig. 1(b and c), respectively. It is found that the model of 6-6 shows similar PCF with a split in the first peak at low temperature to the KA model.[28] The increase of interaction stiffness has two major effects on the PCF of the models. First, the split in the first peaks becomes more significant and the sub-peaks become sharper. This is because the potential energy wells become narrower with an increase of atomic interaction stiffness, which has a stronger confinement effect on atoms located near the energy minima. Second, the peak positions move to larger distance as a increases. As the samples are prepared in the NVT ensemble with pressure of 1, the volumes of these models depend mostly on the repulsive part of potential energy. Hence the increase of steepness in the repulsive part of potential energy shifts peak positions towards a larger distance. Although differences in the PCFs are obvious, the overall structures of these models remain quite similar, due to the same depth and distance of energy minima. Voronoi analysis also shows that these samples have very similar local atomic structures (see Fig. S1, ESI†). This is crucial in this study, because the significant difference in local atomic structures may introduce more complex effects on low-temperature relaxation. Here, to investigate the relation between interatomic potentials and the relaxation behavior far below T_g, we try to reduce the influence of other factors, particularly the effect introduced by structural differences.

B. Internal friction

Although the loss modulus E'' is most commonly used to identify β-relaxation experimentally, the phase difference δ, which can also be interpreted as $\tan(\delta) = E''/E$, is used in this study to reveal the internal friction in the models.[29] In the studied models, change of interaction stiffness strongly affects the shear modulus E, and hence the loss modulus E'', therefore it is inappropriate to compare the internal friction by E''. Phase difference δ, on the other hand, measures relation between elasticity and viscosity as temperature changes, regardless of the change of modulus E (see Fig. S2, ESI†). Fig. 2 shows the internal friction δ of these models measured by the MD-DMA simulations. It can be seen that steepening in both the attractive part and repulsive part of atomic potentials increases the internal friction. Such effect is most significant when both parts in atomic potentials are changed together. The increase of internal friction means that more energies are dissipated during the MD-DMA processes. The results indicate that the low-temperature relaxation dynamics in an amorphous system is enhanced as the atomic interaction stiffness increases.

C. Atomic displacement analysis

To understand the underlying mechanism that causes the differences in low-temperature relaxation among these models,
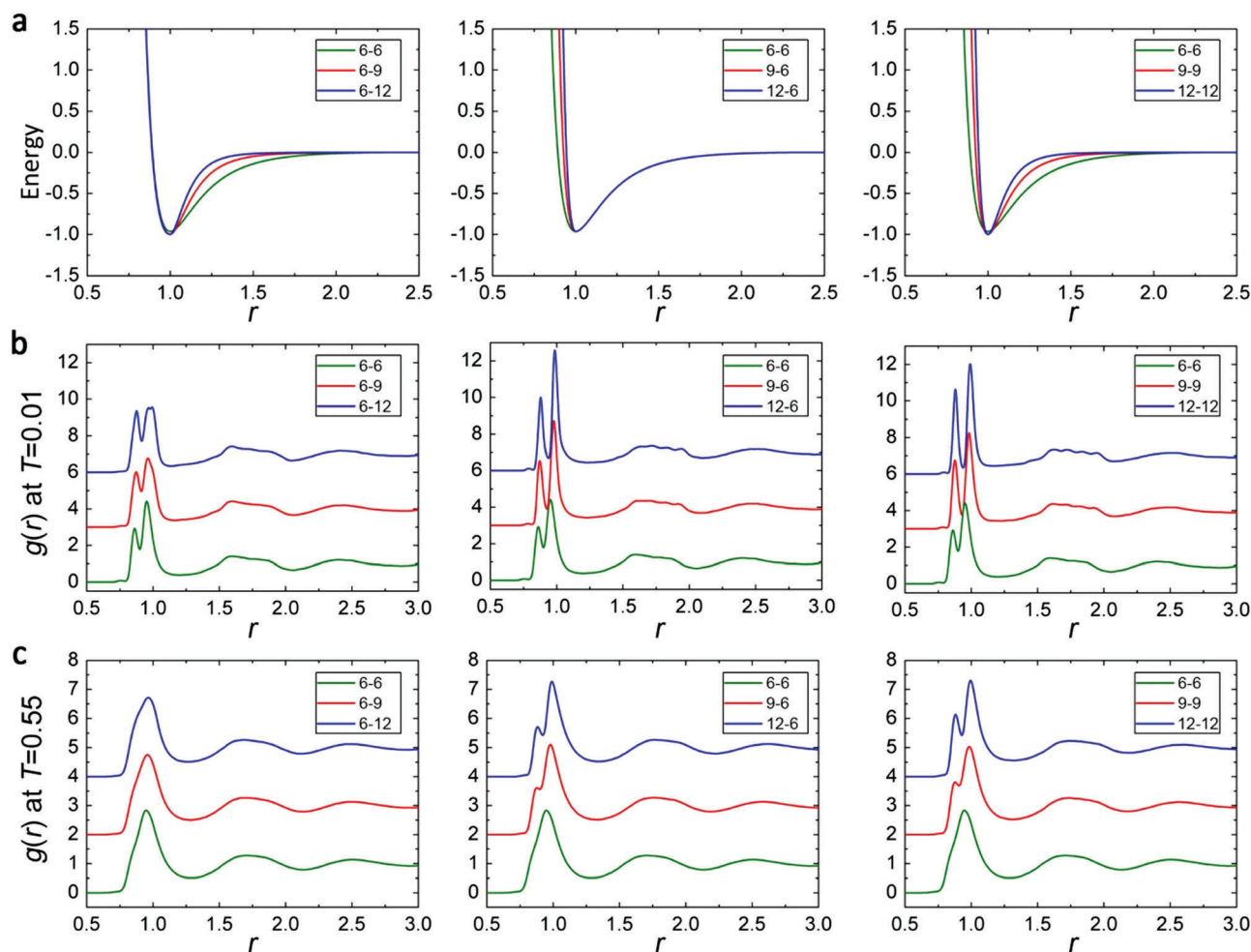
Fig. 1 The interatomic potential and the corresponding pair correlation function. (a) The interatomic potentials of A atoms as a function of reduced distance r in models of 6-6, 6-9, 6-12, 9-6, 12-6, 9-9, 12-12, respectively. The width of potential well indicates the stiffness of atomic interaction. The pair correlation functions for the corresponding models at $T = 0.01$ (b) and $T = 0.55$ (c) in supercooled liquid region, respectively. The change in $g(r)$, as interaction stiffness increases, is insignificant, with slightly sharper and right shifted peaks.

we calculated the atomic displacement $u = \mathbf{r}_i(t + T_\omega) - \mathbf{r}_i(t)$ for each atom during each time period T_ω in the MD-DMA processes. Fig. 3(a) shows the distribution $p(u)$ of atomic displacement u for model 6-6 at various temperatures, normalized by the peak positions and heights, respectively. It was found that the distributions of u on the left side at different temperatures follow Gaussian distribution. On the right side, however, distributions of u deviate from Gaussian distribution, and vary with temperature. At temperatures below 0.31, the distributions have similar shapes. As temperature increases, the deviation increases and reaches its maximum at $T = 0.43$, which is close to T_g of the model. As temperature further increases, distribution of u in the supercooled region becomes closer to Gaussian distribution again.

Since the major difference in the distribution of u at different temperatures is the deviation from Gaussian distribution, which indicates that mobile atoms may have great impact on the low-temperature relaxation dynamics, it is important to study the effect of highly mobile atoms on relaxation process. In a single MD-DMA process, 40 cycles were performed, so that

the atomic displacement u in each cycle contained both vibrational and diffusive motions. In this sense, the total atomic displacement of each atom in the whole MD-DMA process is not suitable to evaluate the atomic mobility in the relaxation process. Here, we considered the atoms with 5% largest atomic displacements u in each cycle to be 'activated atoms', so that the number of activated times n of each atom in the entire MD-DMA process of 40 cycles can be used to evaluate atomic mobility. Fig. 3(b) shows probability distribution $p(n)$ of the activation times n for model 6-6 at various temperatures. Obvious difference can be seen in the distribution of n at low and high temperatures. The distribution of $p(n)$ at high temperatures is close to random distribution. However, at low temperatures, $p(0)$ is much larger, which indicates that most atoms are not activated and remain stable in the entire MD-DMA process. In addition, as n is larger than 5, $p(n)$ is larger than random distribution again as shown in the inset in Fig. 3(b), indicating that a number of atoms remain highly mobile in the MD-DMA process. This demonstrates that the low-temperature relaxation dynamics is heterogeneous. Such dynamical heterogeneity
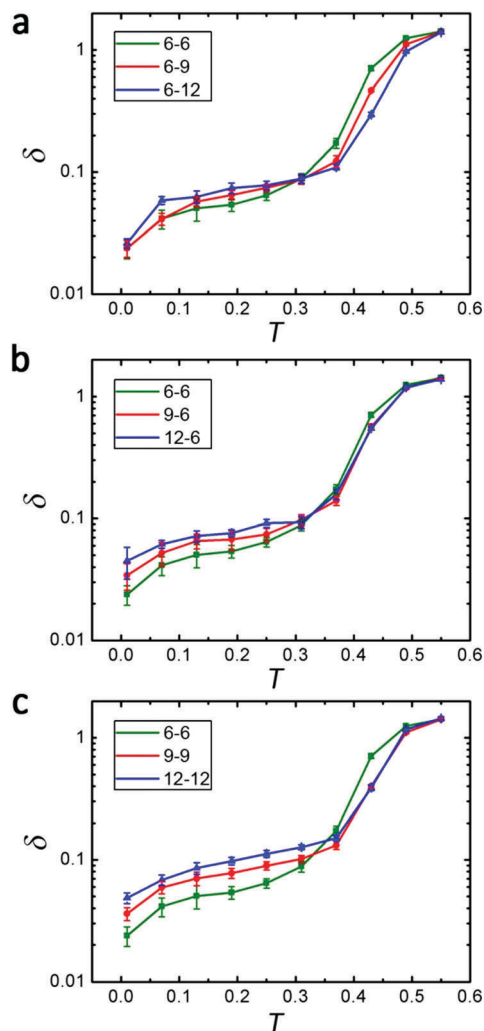
Fig. 2 The internal friction measured by MD-DMA. (a–c) The internal frictions for models with different attractive interactions, repulsive interactions and both attractive and repulsive interactions, respectively. Low-temperature relaxation dynamics is enhanced with the increase of interaction stiffness.
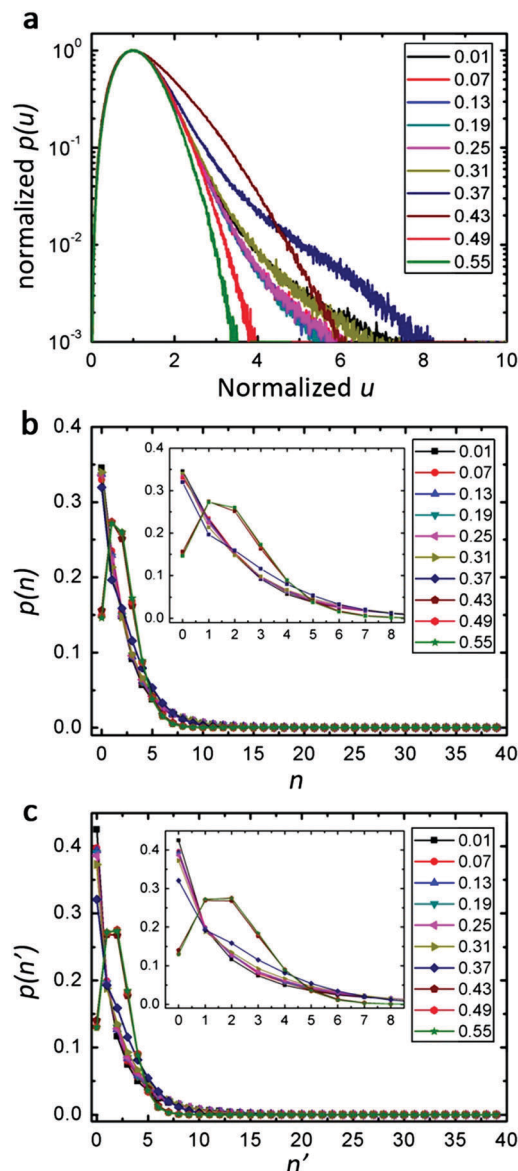

Fig. 3 The atomic displacement analysis for different models. (a) The normalized distribution $p(u)$ of atomic displacement u for model 6-6 at different temperatures, which indicates the evolution of dynamical heterogeneity with temperature. (b) The distribution of atoms with different activated times n (selected by top 5% atoms with the largest displacements u) for model 6-6. Inset: Zoomed-in of the main figure in smaller n. (c) The distribution of atoms with different activated times n'. Here the activated atoms were defined by the top 5% atoms with the largest non-affine displacement D^2. Inset: Zoomed-in of the main figure in smaller n'.

is believed to have great impact on the relaxation dynamics of amorphous materials.[15,30,31]

To confirm the suitability of the activation time n for evaluating the atomic mobility, we also adopted the non-affine displacement D^2 of each atom instead of atomic displacement u[32] (see Fig. S3, ESI†). We selected atoms with the largest 5% of D^2 in each cycle to be 'activated atoms', and the corresponding distribution $p(n')$ is shown in Fig. 3(c). It can be seen that the probability distribution $p(n')$ of activated times n' calculated from these two methods are similar, indicating the universal feature of the distribution in MD-DMA process. Therefore, we simply use atomic displacement u to characterize the activation times of each atom in MD-DMA process. Here, only the data of model 6-6 is shown, since all models with different interacting potentials share similar patterns in the distributions of $p(u)$ and $p(n)$ at different temperatures.

The differences in low-temperature relaxation among different models were analyzed by the distribution of n, as an indicator of

atomic mobility. Since the distributions of n are similar in the temperature range of 0.07 and 0.31, the data within this temperature range were averaged to present the dynamics at low temperatures. Fig. 4(a–c) shows the distribution of n of different models at low temperatures, respectively. As the atomic interaction stiffness increases, the probability $p(0)$ of an atom to remain stable throughout the entire MD-DMA process increases. Furthermore, the probability $p(n > 5)$ also increases with increasing of interaction stiffness, no matter whether the repulsive part and the
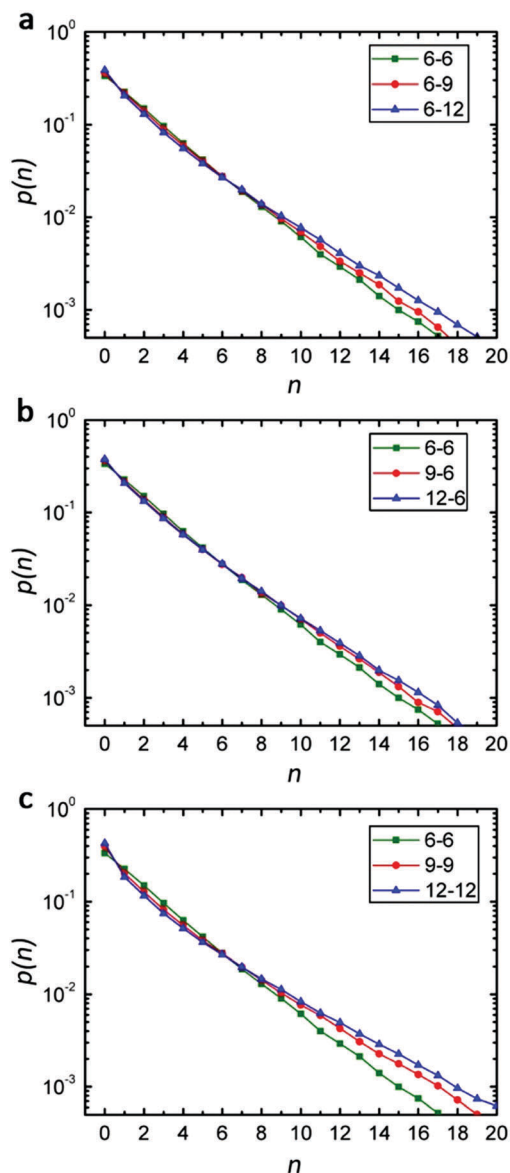
Fig. 4 The dynamical heterogeneity in different models. The distribution of atoms with different activated times n, averaged over the temperature range of 0.07 and 0.31, for models with different attractive interactions (a), repulsive interactions (b) and both attractive and repulsive interactions (c). The increase of interaction stiffness enhances the dynamical heterogeneity at low temperatures.

attractive part are changed separately or simultaneously. Thus, the increase of interaction stiffness enhances the difference between mobile and immobile atoms, and makes the relaxation dynamics more heterogeneous in amorphous materials. The more heterogeneous the dynamics is in glassy materials, the larger the internal friction is, as shown in Fig. 2, and thus the more significant the low-temperature relaxation is. Therefore, dynamical heterogeneity may be responsible for the low-temperature relaxation in glassy materials.

D. Spatial distribution of dynamical heterogeneity

To further understand the dynamical heterogeneity in glassy materials the spatial distribution of activation times n for each

atoms was investigated. Fig. 5(a) shows the atomic configurations of models of 6-6, 9-9, and 12-12 (from left to right) at $T = 0.25$ with atoms colored according to the activated times n, respectively. It is obvious that atoms with larger mobility have a tendency to locate close to each other. As $T = 0.55$, however, the dynamics becomes much more homogeneous, as shown in Fig. 5(b) for model 6-6. To further illustrate the difference of dynamical heterogeneity in these models with increasing interaction stiffness, only atoms with $n > 10$ in model 6-6, 9-9, and 12-12 at $T = 0.25$ were shown in Fig. 5(c), corresponding to the similar atomic configurations in Fig. 5(a). As shown in Fig. 5(c), a significant increase of atoms with $n > 10$ can be observed with the increase of interaction stiffness. The number of atoms with $n > 10$ in model 6-6 is 139. It increases to 171 and 251 in model 9-9 and 12-12, respectively. The number increase of highly mobile atoms is strongly correlated to enhancement of low-temperature relaxation dynamics in the MD-DMA process. Such a correlation is consistent with current understanding of the relation between dynamical heterogeneity and relaxation.[10]

To evaluate the length scale of the dynamical heterogeneity at low temperatures, we employed a spatial correlation function of the activation times of atoms

$$F(n, r) = \left. \frac{\langle (n_i - \bar{n})(n_j - \bar{n}) \rangle}{\sqrt{\langle (n_i - \bar{n})^2 \rangle \langle (n_j - \bar{n})^2 \rangle}} \right|_{r = |\mathbf{d}_j - \mathbf{d}_i|}. \quad (2)$$

In eqn (2), $\langle \rangle$ denotes the average over all atom pairs with $r = |\mathbf{d}_j - \mathbf{d}_i|$, and $\bar{n}$ is the mean value of n. As shown in Fig. 5(d), the activation times of atoms show strong correlation in a short distance, and the correlation decreases rapidly to zero as the distance goes beyond 5, which is approximately the length of 5 particles, regardless of the change in interatomic potentials. Our results suggest a universal length scale of dynamical heterogeneity in these glassy systems.

Although its characteristic length scale and time scale is still unclear, dynamical heterogeneity at low temperatures is believed to be an intrinsic property of glassy material, which has strong influence on the relaxation and mechanical properties.[15,33,34] There have been massive studies to measure or calculate the length scale of dynamical heterogeneity at low temperature, which is usually termed as size of shear transformation zones (STZs).[35,36] The previous results indicate that the size of such activation units falls within hundreds of atoms, with minor differences between different compositions or different methods.[37–41] Our MD simulation results indicate a universal length scale of dynamical heterogeneity, with the change of atomic interaction stiffness, which is consistent with the previous studies by Johnson and Samwer.[38,42]

The increase of atomic interaction stiffness increases the confinement of neighbor atoms, as shown in the pair distribution function in Fig. 1. Under the same applied shear strain within the elastic limit, maximum of 2% in this study, the systems undergo similar overall atomic displacements. For models with larger interaction stiffness, stronger shear stress is needed for the same atomic displacement, which is shown in

This journal is © the Owner Societies 2016

Phys. Chem. Chem. Phys., 2016, **18**, 26643–26650 | **26647**
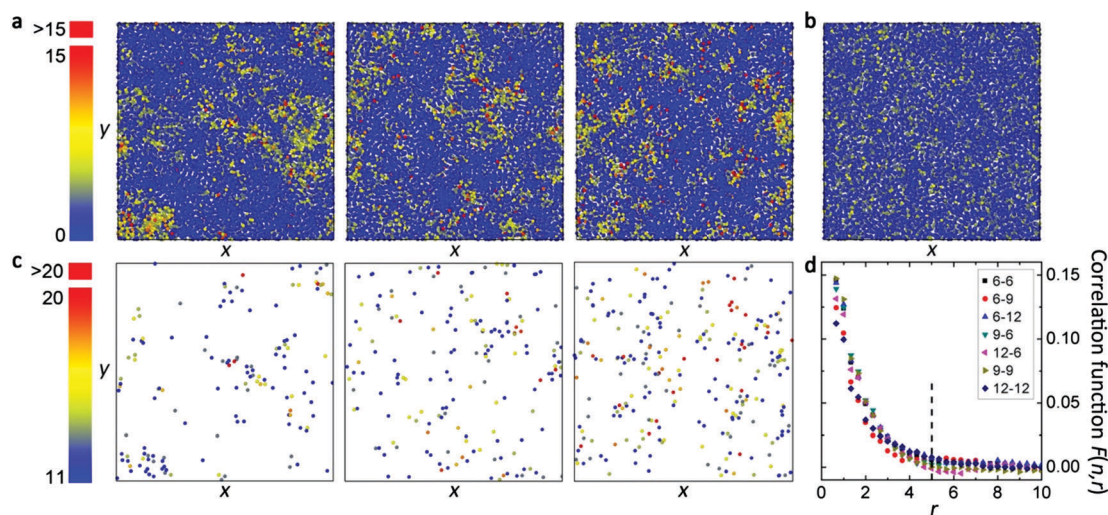
Fig. 5 Spatial heterogeneity of different models. (a) 2D slices of atomic configuration with color code on each atom representing the activated times n. From left to right: model 6-6, 9-9, 12-12 at the $T = 0.25$. (b) 2D slice of atomic configuration of model 6-6 at $T = 0.55$. Dynamical heterogeneity disappears when entering supercooled liquid region. (c) 2D slices of atomic configuration of atoms with $n > 10$ at $T = 0.25$, for model 6-6, 9-9, 12-12, from left to right respectively. As the interaction stiffness increases, the number of highly mobile atoms increases, and the dynamics becomes more heterogeneous. (d) Correlation function $F(n,r)$ for all studied models at $T = 0.25$. A universal length scale of spatial heterogeneity is found in all models with a length of approximately the length of 5 particles.

the increase of shear modulus E. Also, the narrow down of potential clearly indicates that more atoms are likely to dissipate energy in the same displacement. This is directly related to the increase of internal friction at low temperatures. The ability of an atom to dissipate energy is illustrated by its displacements during each loading cycle, or the number of times to be 'activated atoms'. We can see that the stiffening of interactions not only increases difference between the mobile atoms and the matrix, but also increases the number of mobile atoms, which significantly contributes to low-temperature relaxation in glassy materials.

Note that due to the different potential stiffness, different models have different enthalpy states, which might also affect the behavior of β-relaxation in these systems, if the different models relax to states with similar enthalpy values. However, this is not the case in our study, because the enthalpies in these systems change little in MD-DMA simulation processes, and do not relax to similar values, so this effect on the behavior of β-relaxation can be neglected.

IV. Atomic interaction stiffness of metallic glasses

It has been experimentally observed that there is a universal power law relation between bulk modulus K and the averaged molar volume V_m for most metallic glasses and metallic crystalline solids.[43,44] Such relation is believed to originate from short range atomic bonding, rather than long range atomic packing. The relation between K and V_m can be understood by assuming a simple model for atomic interaction:

$$E = 4\varepsilon \left[\left(\frac{\sigma}{r} \right)^n - \left(\frac{\sigma}{r} \right)^m \right], \tag{3}$$

which is similar to the models in our MD simulations. Since the molar volume can be expressed as $V_m \sim N_A \times r^3$, the potential energy of the system can be derived as

$$U = 2\varepsilon \left[\frac{\sigma^n \times N_A^{1+n/3}}{V_m^{n/3}} - \frac{\sigma^m \times N_A^{1+m/3}}{V_m^{m/3}} \right], \tag{4}$$

where N_A is the Avogadro constant. An equilibrium system rests at local energy minima U_0 where $\partial U_0 / \partial V_m = 0$, also, the bulk modulus K can be expressed as $K = V_m \frac{\partial^2 U}{\partial V_m^2} \Big|_{V_m}$. Thus, one can obtain

$$K V_m^\alpha = C, \tag{5}$$

where $\alpha = -(1 = m/3)$, for $C = 2\varepsilon\sigma^m N_A^{1+m/3}(n-m)m/9$; or $\alpha = (1 + n/3)$, for $C = 2\varepsilon\sigma^n N_A^{1+n/3}(n-m)n/9$. In eqn (5), the parameter α indicates the atomic interaction stiffness, which can be determined by the relation between bulk modulus K and average molar volume V_m.

For a broad range of materials, atomic interaction stiffness remains in a relatively small range, so that C in eqn (5) can be considered as a constant. Therefore, the bulk modulus and averaged molar volume follows a power law relation for most materials with $\alpha \sim -2.3$.[44] However, when considering each series of MGs separately, it is found that MGs with different based elements generally follow a power law relation but with a significantly different exponent α. Fig. 6 shows the bulk modulus K *vs.* averaged molar volume V_m for Pd, Cu, Zr, and RE-based MGs (see Table S1, ESI†). Here, Cu- and Zr-based MGs are considered as one series because most MGs in this series consists of both Cu and Zr atoms, and we can see that the data fall in a linear region in a log–log plot. The RE-based MGs are considered as one series for a similar reason. RE-based MGs are found to share many properties, including elastic, thermal,
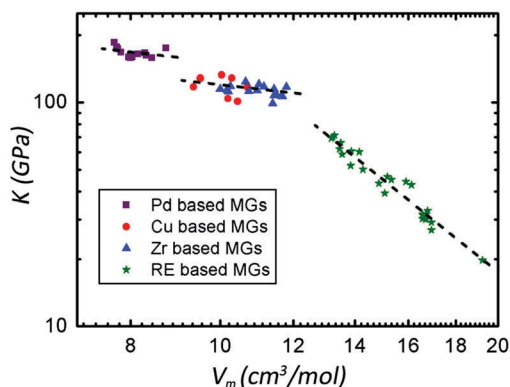
26648 | *Phys. Chem. Chem. Phys.*, 2016, **18**, 26643–26650

This journal is © the Owner Societies 2016

Fig. 6 Bulk modulus (K) vs. average molar volume (V_m) for various Pd, Zr, Cu and RE based MGs. The distributions of data from different groups of MGs follow power law relation, which are fitted by dotted lines in the log–log plot. The much steeper distribution of RE based MGs indicates a stiffer atomic interaction.

and magnetic properties, owing to their similar electronic structures.[45] In these series of MGs, a much steeper decay of K in the log–log plot is found in RE-based MGs, compared to other MGs, which indicates a much larger stiffness of atomic interaction, consistent with the above simulation results.

Although β-relaxation is widely believed to be one of the most fundamental relaxation mechanisms of MGs, prominent β-relaxation peaks in DMS are only found in very limited compositions of MGs, typically RE based MGs.[11,18,19] It is generally accepted that RE-based MGs possess stronger low-temperature relaxation dynamics, whether it is shown as peaks, shoulders, or excess wings in the DMS. Based on the above MD simulation results, we believe that such a phenomenon is caused by the much larger atomic interaction stiffness in RE-based MGs. As the MD simulation results show, increase of interaction stiffness leads to stronger low-temperature relaxations, accompanied by an increase in the intensity of dynamical heterogeneity.

V. Conclusion

The mechanism that controls low-temperature relaxation of glassy materials was investigated *via* MD simulations using models with different atomic interaction stiffness. The results show that the low-temperature relaxation is enhanced by an increase of interaction stiffness. The stiffening of atomic interaction increases the number of highly mobile atoms, which are more likely to dissipate energy during sinusoidal strain, and hence contribute to the internal friction at low temperature. The atomic interaction stiffness of MGs can be estimated experimentally by the relation between the bulk modulus and the averaged molar volume, where RE-based MGs are found to have much stiffer atomic interactions. This could be the underlying mechanism that causes the much stronger β-relaxation in RE-based MGs. The physical picture of low-temperature relaxation from local atomic interaction to dynamical heterogeneity, and eventually to the internal friction of the whole system, may provide better understanding of the dynamical properties of amorphous solids.

References

1 K. L. Ngai and M. Paluch, *J. Chem. Phys.*, 2004, **120**, 857–873.

2 H. B. Yu, W. H. Wang and K. Samwer, *Mater. Today*, 2013, **16**, 183–191.

3 M. Daraktchiev, E. K. H. Salje, W. T. Lee and S. A. T. Redfern, *Phys. Rev. B: Condens. Matter Mater. Phys.*, 2007, **75**, 134102.

4 M. P. Wolcott, S. Z. Yin and T. G. Rials, *Compos. Interfaces*, 2000, **7**, 3–12.

5 P. G. Debenedetti and F. H. Stillinger, *Nature*, 2001, **410**, 259–267.

6 J. Sjostrom, J. Mattsson, R. Bergman, E. Johansson, K. Josefsson, D. Svantesson and J. Swenson, *Phys. Chem. Chem. Phys.*, 2010, **12**, 10452–10456.

7 E. Kaminska, M. Tarnacka, O. Madejczyk, A. Chrobok, K. Kaminski and M. Paluch, *Phys. Chem. Chem. Phys.*, 2016, **18**, 8901–8910.

8 S. Hensel-Bielowka, J. R. Sangoro, Z. Wojnarowska, L. Hawelek and M. Paluch, *Phys. Chem. Chem. Phys.*, 2013, **15**, 9300–9307.

9 W. H. Wang, *J. Appl. Phys.*, 2011, **110**, 053521.

10 Z. Lu, W. Jiao, W. H. Wang and H. Y. Bai, *Phys. Rev. Lett.*, 2014, **113**, 045501.

11 H. B. Yu, W. H. Wang, H. Y. Bai and K. Samwer, *Natl. Sci. Rev.*, 2014, **1**, 429–461.

12 Y. H. Liu, T. Fujita, D. P. B. Aji, M. Matsuura and M. W. Chen, *Nat. Commun.*, 2014, **5**, 163–180.

13 H. B. Yu, K. Samwer, Y. Wu and W. H. Wang, *Phys. Rev. Lett.*, 2012, **109**, 095508.

14 H. Tanaka, *Phys. Rev. E: Stat., Nonlinear, Soft Matter Phys.*, 2004, **69**, 021502.

15 Y. Fan, T. Iwashita and T. Egami, *Nat. Commun.*, 2014, **5**, 5083.

16 Z. F. Zhao, P. Wen, C. H. Shek and W. H. Wang, *Phys. Rev. B: Condens. Matter Mater. Phys.*, 2007, **75**, 174201.

17 H. B. Yu, K. Samwer, W. H. Wang and H. Y. Bai, *Nat. Commun.*, 2013, **4**, 1345–1346.

18 Z. G. Zhu, Y. Z. Li, Z. Wang, X. Q. Gao, P. Wen, H. Y. Bai, K. L. Ngai and W. H. Wang, *J. Chem. Phys.*, 2014, **141**, 084506.

19 Z. G. Zhu, Z. Wang and W. H. Wang, *J. Appl. Phys.*, 2015, **118**, 154902.

20 Z. Wang, H. B. Yu, P. Wen, H. Y. Bai and W. H. Wang, *J. Phys.: Condens. Matter*, 2011, **23**, 5919–5926.

21 Y. Cohen, S. Karmakar, I. Procaccia and K. Samwer, *EPL*, 2012, **100**, 36003–36006.

22 D. Bedrov and G. D. Smith, *Phys. Rev. E: Stat., Nonlinear, Soft Matter Phys.*, 2005, **71**, 050801.

This journal is © the Owner Societies 2016

Phys. Chem. Chem. Phys., 2016, **18**, 26643–26650 | 26649

23 S. Karmakar, C. Dasgupta and S. Sastry, *Phys. Rev. Lett.*, 2016, **116**, 085701.

24 W. Kob and H. C. Andersen, *Phys. Rev. E: Stat., Nonlinear, Soft Matter Phys.*, 1995, **52**, 4134–4153.

25 W. Kob and J. L. Barrat, *Phys. Rev. Lett.*, 1997, **78**, 4581–4584.

26 H. B. Yu and K. Samwer, *Phys. Rev. B: Condens. Matter Mater. Phys.*, 2014, **90**, 144201.

27 H. B. Yu, R. Richert, R. Maass and K. Samwer, *Nat. Commun.*, 2015, **6**, 7179.

28 U. R. Pedersen, T. B. Schroder and J. C. Dyre, *Phys. Rev. Lett.*, 2010, **105**, 157801.

29 M. S. Blanter, I. S. Golovin, H. Neuhauser and H. R. Sinning, *Materia Japan*, 1986, **25**, 624–632.

30 Y. Z. Li, L. Z. Zhao, C. Wang, Z. Lu, Y. Bai and W. H. Wang, *J. Chem. Phys.*, 2015, **143**, 041104.

31 Y. C. Hu, F. X. Li, M. Z. Li, H. Y. Bai and W. H. Wang, *Nat. Commun.*, 2015, **6**, 8310.

32 M. L. Falk and J. S. Langer, *Phys. Rev. E: Stat., Nonlinear, Soft Matter Phys.*, 1998, **57**, 7192–7205.

33 J. Ding, S. Patinet, M. L. Falk, Y. Q. Cheng and E. Ma, *Proc. Natl. Acad. Sci. U. S. A.*, 2014, **111**, 14052–14056.

34 H. Tanaka, T. Kawasaki, H. Shintani and K. Watanabe, *Nat. Mater.*, 2010, **9**, 324–331.

35 H. Sillescu, R. Bohmer, G. Diezemann and G. Hinze, *J. Non-Cryst. Solids*, 2002, **307**, 16–23.

36 W. H. Jiang, H. H. Liao, F. X. Liu, H. Choo and P. K. Liaw, *Metall. Mater. Trans. A*, 2008, **39A**, 1822–1830.

37 S. G. Mayr, *Phys. Rev. Lett.*, 2006, **97**, 195501.

38 M. Zink, K. Samwer, W. L. Johnson and S. G. Mayr, *Phys. Rev. B: Condens. Matter Mater. Phys.*, 2006, **73**, 172203.

39 D. Pan, A. Inoue, T. Sakurai and M. W. Chen, *Proc. Natl. Acad. Sci. U. S. A.*, 2008, **105**, 14769–14772.

40 M. L. Manning, E. G. Daub, J. S. Langer and J. M. Carlson, *Phys. Rev. E: Stat., Nonlinear, Soft Matter Phys.*, 2009, **79**, 016110.

41 S. T. Liu, Z. Wang, H. L. Peng, H. B. Yu and W. H. Wang, *Scr. Mater.*, 2012, **67**, 9–12.

42 W. L. Johnson and K. Samwer, *Phys. Rev. Lett.*, 2005, **95**, 195501.

43 J. Q. Wang, W. H. Wang, H. B. Yu and H. Y. Bai, *Appl. Phys. Lett.*, 2009, **94**, 121904.

44 M. Q. Jiang, G. Wilde, J. B. Gao and L. H. Dai, *Scr. Mater.*, 2013, **69**, 760–763.

45 Q. Luo and W. H. Wang, *J. Non-Cryst. Solids*, 2009, **355**, 759–775.